Echocardiographic assessment of left bundle branch–related strain dyssynchrony

Ultrasound in Med. & Biol., Vol. 45, No. 8, pp. 2063–2074, 2019

0301-5629/$ - see front matter

https://doi.org/10.1016/j.ultrasmedbio.2019.03.012

● *Original Contribution*

ECHOCARDIOGRAPHIC ASSESSMENT OF LEFT BUNDLE BRANCH–RELATED STRAIN DYSSYNCHRONY: A COMPARISON WITH TAGGED MRI

Louis S. Fixsen,* Anouk G.W. de Lepper,† Marc Strik,‡ Lars B. van Middendorp,‡ Frits W. Prinzen,‡ Frans N. van de Vosse,* Patrick Houthuizen,† and Richard G.P. Lopata*

* Cardiovascular Biomechanics, Department of Biomedical Engineering, Eindhoven University of Technology, Eindhoven, The Netherlands; † Department of Cardiology, Catharina Hospital, Eindhoven, The Netherlands; and ‡ Department of Physiology, Cardiovascular Research Institute Maastricht, University of Maastricht, Maastricht, The Netherlands

(*Received* 24 *July* 2018; *revised* 22 *March* 2019; *in final from* 25 *March* 2019)

Abstract—Recent studies have shown the efficacy of myocardial strain estimated using speckle tracking echocardiography (STE) in predicting response to cardiac resynchronisation therapy. This study focuses on circumferential strain patterns, comparing STE-acquired strains to tagged-magnetic resonance imaging (MRI-T). Second, the effect of regularisation was examined. Two-dimensional parasternal ultrasound (US) and MRI-T data were acquired in the left ventricular short-axis view of canines before (n = 8) and after (n = 9) left bunch branch block (LBBB) induction. US-based strain analysis was performed on Digital Imaging and Communications in Medicine data at the mid-level using three overall methods ("Commercial software," "Basic block-matching," "regularised block-matching"). Moreover, three regularisation approaches were implemented and compared. MRI-T analysis was performed using SinMod. Normalised regional circumferential strain curves, based on standard six or septal/lateral segments, were analysed and cross-correlated with MRI-T data. Systolic strain (SS) and septal rebound stretch (SRS) were calculated and compared. Overall agreement of normalised circumferential strain was good between all methods on a global and regional level. All STE methods showed a bias (≥4% strain) toward higher SS estimates. Pre-LBBB, septal and lateral segment correlation was excellent between the Basic (mean $\rho = 0.96$) and regularised (mean $\rho = 0.97$) methods and MRI-T. The Commercial method showed a significant discrepancy between the two walls (septal $\rho = 0.94$, lateral $\rho = 0.68$). Correlation with MRI-T reduced between pre- and post-LBBB (Commercial $\rho = 0.79$, Basic $\rho = 0.82$, mean regularised $\rho = 0.86$). Septal strain patterns and SRS varied with the STE software and type of regularisation, with all STE methods estimating non-zero SRS values pre-LBBB. Absolute values showed moderate agreement, with a bias for higher strain from STE. SRS varied with the type of software and extra regularisation applied. Open efforts are needed to understand the underlying causes of differences between STE methods before standardisation can be achieved. This is particularly important given the apparent clinical value of strain-based parameters such as SRS. (E-mail: l.s.fixsen@tue.nl)

Key Words: **Echocardiography, LBBB, Dyssynchrony, Speckle tracking, Regularisation.**

INTRODUCTION

Left bundle branch block (LBBB) leads to mechanical dyssynchrony resulting in reduced cardiac performance. Despite the success of cardiac resynchronisation therapy (CRT) in these patients (McMurray et al. 2012), it remains challenging to identify optimal inclusion criteria for CRT candidates, with the percentage of non-responders between 20% and 40% (Holzmeister et al. 2011). Current guidelines focus on the electrical substrate and state that a patient should have an elongated QRS complex and a left ventricular (LV) ejection fraction ≤35% to be considered for CRT (Brignole et al. 2013).

Numerous echocardiographic techniques have been used to predict CRT response by quantifying mechanical dyssynchrony. Most techniques use timing indices to estimate dyssynchrony, acquired using tissue Doppler imaging (TDI), pulsed Doppler or speckle tracking

Address correspondence to: Louis S. Fixsen, Cardiovascular Biomechanics, Department of Biomedical Engineering, Eindhoven University of Technology, P.O. Box 513, 5600 MB Eindhoven, The Netherlands. E-mail: l.s.fixsen@tue.nl

echocardiography (STE) (Achilli et al. 2006; Ghani et al. 2015). However, the large PROSPECT trial showed that these indices had little predictive ability (Chung et al. 2008).

Other indices based on strain amplitude or patterns have been proposed, estimated using tagged-magnetic resonance imaging (MRI-T) (Kirn et al. 2008), and more recently, STE (De Boeck et al. 2009). Studies have shown the possible predictive value of STE-based strain (Maréchaux et al. 2014; Risum et al. 2012), global longitudinal strain (GLS) (D'Andrea et al. 2009) and activation pattern (Bunting et al. 2016). Although MRI-T has been successfully used in the estimation of mechanical dyssynchrony, routine clinical use of MRI-T has been precluded by complex acquisition protocols, processing and high costs. In contrast, STE can be performed on data acquired as part of a standard echocardiographic exam, although expertise is needed in processing and interpretation.

Despite numerous improvements since STE's introduction, the technique still suffers from a lack of standardisation (Badano et al. 2013). Progress has been made recently with a taskforce established to correct this (Voigt et al. 2015), with a focus on GLS (D'hooge et al. 2016). Problems in standardisation stem partially from the closed nature of commercial software. The exact methods used by the software in strain estimation and regularisation are developed by each vendor and are proprietary information (Singh et al. 2010). Furthermore, some software only use Digital Imaging and Communications in Medicine (DICOM) acquired using the vendor's hardware, making direct comparisons cumbersome. Although early publications for some software are available (Rappaport et al. 2006), development of these software has continued in the intervening years.

Thus far, the majority of LBBB strain analysis research using STE has been performed on longitudinal strain. This is due to its lower inter- and intra-observer and inter-vendor variability, compared with circumferential or radial strain (Badano et al. 2013). However, circumferential strain has been shown to be more sensitive to dyssynchrony than longitudinal strain (Helm et al. 2005). In addition, circumferential strain may enable detailed analysis of septal strain patterns (Han et al. 2010). Interestingly, a recent study comparing circumferential strain patterns obtained using STE in LBBB patients found poor agreement between commercial STE software and MRI-T (van Everdingen et al. 2018). We hypothesised that this poor agreement could be due to elements of the software (regularisation for example), rather than problems with STE itself.

Therefore, in this study we further examined the feasibility and value of STE-based circumferential strain for LBBB identification in a validation with MRI-T. Similarities of regional strain patterns were assessed in the myocardium of canines before and after LBBB, using both academic and commercial STE algorithms. Furthermore, we determined the key limiting factors precluding the use of circumferential strain in the assessment of LBBB-type contraction patterns.

METHODS

Canines

A previously acquired data set of two-dimensional B-mode ultrasound (US) and MRI-T images in 13 adult mongrel dogs of either sex and unknown age was used in this study (Strik et al. 2013). This data set included images of the left ventricle before (pre-LBBB, n = 8) and after (post-LBBB, n = 9) LBBB was induced. Anaesthesia was induced using pentothal and maintained through intravenous infusion of midazolam (0.25 mg/kg/h) and sufentanil (3 μg/kg/h). LBBB was created through radiofrequency ablation of the proximal left bundle branch within the basal septum, thus inducing dyssynchronous activation of the septal and posterolateral wall. Animal handling was performed according to the Dutch Law on Animal Experimentation and the European Directive for the Protection of Animals Used for Scientific Purposes (Directive 2010/63/EU). The protocol was approved by the Animal Experimentation Committee of Maastricht University.

Right ventricular (RV) and LV pressures were measured simultaneously with manometer tipped catheters positioned in each ventricle. Surface electrocardiogram (ECG) was acquired *via* limb leads. Inter-ventricular mechanical dyssynchrony (IVMD) was derived from ventricular pressure and ECG (Verbeek et al. 2002). LV end-diastolic and end-systolic dimensions were calculated from biplane cine MRI images.

MRI-T

Sequences of cine and MRI-T images were acquired using a 1.5 T Philips Intera MRI scanner (Philips Healthcare, Best, The Netherlands), in combination with a sensitivity encoding (SENSE) cardiac coil, at a temporal resolution of 15 ms. MRI-T images were acquired with a prospectively triggered gradient echo planar imaging sequence, yielding short-axis views at seven points along the LV from apex to base, with both horizontal and temporal tag line patterns. Each acquisition was terminated after 540 ms due to the dispersion of tag lines. Endpoints of acquisitions varied between mid-diastole and end-diastole because of differences in heart rate. Magnetic resonance imaging (MRI) and US data were acquired on the same day.

MRI data were analysed using SinMod (Maastricht University, Maastricht, The Netherlands) (Arts et al. 2010),

an MRI-T displacement estimation toolbox implemented in MATLAB (MATLAB version 9.2, 64-bit, The Mathworks Inc., Natick, MA, USA). For each short-axis slice, the cavity and epicardium were segmented manually and the posterior and anterior septal insertion of the RV free wall were defined. Slices that included the papillary muscles were selected and displacements within each image were estimated, an example MRI-T image at this level can be seen in Figure 1a. Circumferential strain was calculated based on the displacement maps for each slice and averaged into a single bullseye-style plot. The estimated strain maps were separated into the standard six-segment and a lateral-septal wall arrangement, seen in Figure 1 (b, c).

Ultrasound

Acquisition. Two-dimensional US DICOM images (434 × 636 pixels) were acquired of the canine LV, whilst under anaesthesia, using a GE Vivid5 US machine (GE Vingmed Ultrasound, Norten, Norway). A GE PA2-5 phased array transducer (3-MHz centre frequency, 75-degree opening angle, 90 frames per second) was used to image the short axis of the LV at the level of the papillary muscle. Care was taken to have a high-quality image with a clear endocardial border definition, as seen in Figure 1d.

Speckle tracking. Speckle tracking involves tracking regions of speckle, an interference pattern that occurs when US is reflected by point scatters, the appearance of which is determined by the imaging position and probe. Optical flow techniques such as windowed cross-correlation are able to estimate local changes in the pattern over time and therefore underlying tissue movement. The precision and accuracy of these techniques are heavily dependent on frame rate and image quality, which can be affected by axial and lateral resolution, the type of US data (radiofrequency or B mode), shadowing and imaging depth. Cardiac applications of speckle tracking are particularly challenging due to the typically poor image quality, as well as the rapid movement and deformation of the heart, both within and outside the imaging plane.

US DICOM data were processed using two speckle tracking methods: in-house developed STE software—"Basic" and commercial software—"Commercial." In order to evaluate the impact and effect of regularisation (through filtering of spatial and temporal data), three techniques were applied to the Basic software: "Median," "Fourier" and "Cubic"; these are explained in "*Regularised methods*." Identical US data were analysed by each speckle tracking method. The Basic algorithm provides the most rudimentary tracking data possible. Next, regularisation was added for spatial and temporal filtering of outliers. Finally, the commercial software was used, known to be heavily regularised although being a "black-box." Many other combinations of commercial and academic software are possible. However, in order to maintain clarity within the present study, these options were selected.

Timing definitions. Mitral valve closure (MVC) was used to define the start and end of each cardiac cycle, *i.e.,* at end diastole (Voigt et al. 2015; Amundsen et al. 2015). For the Basic and regularised methods, corresponding US frames were selected manually. The commercial software did not allow the start point to be selected: data were shortened to the point of MVC afterwards, based on the ECG data.

The end of contraction, end systole, was defined as the point of aortic valve closure (AVC). However, in dyssynchronous hearts, the end of contraction often does not occur at the same time as AVC.

Basic method

The Basic method was implemented in MATLAB, previously described by Lopata et al. (2009). The endocardium and epicardium, just inwards of the

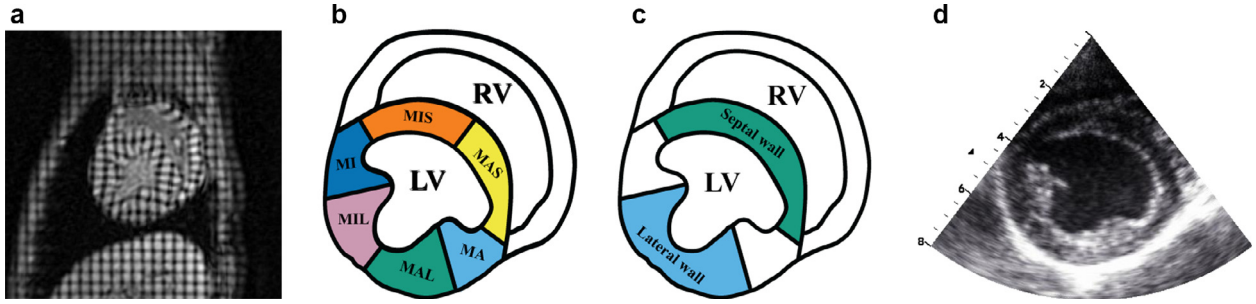

Fig. 1. (a) Example short-axis MRI-T image of a canine heart during mid-systole, with combined vertical and horizontal tag-lines. (b) Six-segment representation: MA, MAL, MIL, MI, MIS, MAS. (c) Lateral and septal wall segments. The right ventricle was not included in the analysis. (d) Example B-mode US image of the canine LV. MRI-T = tagged-MRI; MA, mid-anterior; MAL, mid-anterolateral; MIL, mid-inferolateral; MI, mid-inferior; MIS, mid-inferoseptal; MAS, mid-anteroseptal; RV = right ventricular; LV = left ventricular; US = ultrasound.

pericardium, were manually segmented to generate a mesh of 11 radial and 91 circumferential coordinates around the ventricle wall, *i.e.,* a local coordinate system. The STE method uses "coarse-to-fine" 2-D block matching to calculate the cross-correlation function of windows of image data between frames, and therefore estimate the inter-frame displacements. A large template of B-mode DICOM data (51 × 51 pixels) is used in the first iteration, resulting in a coarse displacement field. These initial displacements are input to the second iteration, where the template is reduced to a quarter of its original size (25 × 25 pixels) and final displacements are obtained. The displacements were then used to track each point of the segmented mesh over the cardiac cycle. Circumferential strain was calculated by taking the spatial derivative of the deformation of the mesh in the circumferential direction, relative to the first frame, using a least-squares strain estimator.

The anterior septal insertion of the RV free wall was defined and strains were averaged into the six segments. Lateral and septal wall strain was calculated by averaging the points within the mid-anterior and mid-inferior lateral and septal segments. Drift compensation was not applied to the Basic or regularised methods.

Regularised methods. Regularisation is a process used in STE software which, in a simple implementation, consists of the filtering and smoothing of results (*i.e.,* estimated displacement) in order to make them both more interpretable and reproducible. More complex implementations aim to regularise the geometry or deformation applied to a geometry based on *a priori* knowledge, which can fail in the case of a severe pathology. An important consideration in implementing regularisation methods is the trade-off between variance and bias within estimates; under-fitting leads to a low variance (*i.e.,* multiple similar estimates) but a higher degree of bias towards incorrect estimates. This is could be because the regularisation does not take the underlying mechanics into account accurately and is too loosely defined. Over-fitting occurs when an algorithm is too rigid to respond to new data. The algorithm will perform very well on training data, but poorly elsewhere.

Regularisation is particularly necessary in the case of 2-D cardiac STE: the geometry specified is observer specific if it is manually segmented; furthermore, the deformation within a 2-D imaging plane is estimated, whilst the heart itself deforms in three dimensions (Badano et al. 2013). Therefore, the through-plane motion of the myocardium is often the greatest source of error in STE. Care must be taken not to over-fit the data however, especially in the instance of dis-coordinated deformation as is the case in hearts with LBBB (Prinzen et al. 1999).

As part of the assessment of circumferential strain, three regularisation approaches were implemented and applied to the results of the Basic method. A windowed-median filter, "Median," was implemented which filtered the estimated per-frame displacements, in the second iteration of the Basic algorithm, with a moving window of 15 × 7 pixels.

The second method, "Fourier," consisted of a Fourier curve-fit of the inner and outer contours of the mesh. The manually segmented contours (x and y coordinates) of the first frame were decomposed into five Fourier coefficients that together describe the geometry as a series of periodic signals. The three high-order coefficients were fixed at their original values for every frame. The two lowest order coefficients were calculated with a least-squares curve fit of the inner and outer contours for each frame. Per-frame tracking points were then calculated by using the resulting fitted and fixed coefficients. Hence, the contours were able to deform, but maintained the initial geometry, reducing the number of errant tracking points. Circumferential strains were estimated based on the deformation of the contours, and averaged into the six segments and the lateral and septal segments.

The third approach, "Cubic," consisted of spatial and temporal cubic spline smoothing (Pollock et al. 1999) of the inner and outer contours of the mesh. This method is used in the Commercial software in conjunction with an image quality-based weighting algorithm (Moen et al. 2013), although the latter was not implemented in this study. Spatial smoothing was applied to the points of the mesh per frame, whilst temporal smoothing was applied to each point in turn over the entire frame series.

Commercial software

Data were loaded into the commercial software (EchoPac PC, version 110.1.7, 2012, GE Vingmed Ultrasound, Norten, Norway). Rather than tracking 2-D blocks of pixels across the whole image, as in the Basic software, the software tracks individual bright features within the image (Rappaport et al. 2006). The start and endpoints of the heart cycle were automatically selected. The LV was manually defined and a region-of-interest (ROI) generated by the software. The ROI was then user adjusted such that it covered the thickness LV wall, inward of the pericardium. After segmentation, the six pre-defined segments were rotated, such that the point between the mid-anterior septum and mid-anterior segment aligned with the anterior septal insertion of the RV free wall (Fig. 1b). The position of each segment was compared to those in the Basic software to ensure alignment between methods. Default settings for temporal filtering, spatial filtering and drift compensation were used

(centre of user-selectable range, no values given, drift compensation was automatically applied).

Statistical analysis

Strain curves were cross-correlated over the matching portions of each cycle to analyse their similarity. Each curve was first normalized by addition of its minimum value and subsequent division by its maximum value, meaning all values were in a range between 0 and 1. STE-estimated curves were down sampled to match the MRI sample rate, resulting in coarser strain curves over time. This did not affect strain estimates as the sample-rate remained sufficient. Because of the differences in timing definitions between the methods, curves of mean strain across all segments were cross-correlated to ensure temporal alignment. Linear correlation (Pearson's) was performed between the aligned segmental strain curves to find the correlation coefficient (ρ). The statistical significance of the change in correlation between segments pre- and post-LBBB was found with a two-tailed two-sample *t*-test (significance level 0.05).

Absolute strain values were compared by calculating systolic strain (SS), *i.e.,* the absolute difference between minimum and maximum mean strain per beat, prior to aortic valve closure (van Everdingen et al. 2017). SS is inclusive of the pre-stretch seen in the lateral wall during LBBB, whereas other parameters such as peak SS exclude this part of the strain pattern. Systolic strain estimates from all STE types were compared to MRI-T through Bland-Altman plots. A flowchart of the overall comparison process can be seen in Figure 2.

Pre- and post-LBBB septal strain patterns were compared through septal rebound stretch (SRS) (De Boeck et al. 2009). SRS was calculated as the sum of systolic stretch post-contraction (MVC) and before AVC. SRS values were compared by calculating the two-tailed Pearson's correlation coefficient (R).

RESULTS

Of the 13 canines, full imaging data were available for four canines both pre- and post-LBBB. Solely pre- and post-LBBB acquisitions were available in four and five canines, respectively. Table 1 shows haemodynamic measurements taken during the pre- and post-LBBB acquisitions. A reduction was found in the magnitude of minimum and maximum LV dP/dt between canines pre- and post-LBBB. IVMD increased in magnitude (average of 33 ms). QRS duration post-LBBB was twice the QRS duration pre-LBBB. The classical threshold of 120 ms for LBBB was not met because the canine heart is much smaller than the human heart, resulting in shorter conduction delays.

Comparison of circumferential strain

Table 2 shows full results of the Pearson's correlation between the normalized segmental strain curves of each STE method and MRI-T. Good correlation with MRI-T is seen across the six segments pre- and post-LBBB, in the majority of cases. Moderate correlation ($\rho = 0.55/0.56$) is seen in the lateral wall segments of the commercial method pre-LBBB, post-LBBB correlation is improved ($\rho = 0.69/0.65$, $p < 0.05$).

Between pre- and post-LBBB, correlation is reduced around the LV for the Basic and regularised methods, with the most pronounced reduction found in the septal segments ($\rho > 0.89 - < 0.81$, $p < 0.05$). All methods show a reduction in correlation after LBBB induction in the septal wall, with the Commercial method having the greatest reduction ($p < 0.05$) and the Cubic method the lowest ($p < 0.05$). The Basic and regularised methods perform similarly to pre-LBBB in the lateral wall with a small reduction in correlation (not significant). Conversely, the Commercial method shows improved correlation with MRI-T in the lateral wall ($p < 0.05$). Correlation of average strain is good for all methods pre- and post-LBBB. Both the Fourier and Cubic methods showed significant improvement in correlation over the Basic method in the septal wall ($p < 0.05$).

Bland-Altman plots of SS pre- and post-LBBB are shown in Figure 3. The Basic and regularised methods have lower differences with MRI-T than the Commercial method, except in the lateral wall post-LBBB. Although the Basic and regularised methods show systematic over-estimation of strain compared to MRI-T (>4% SS), there is greater variability for the Commercial method, except in the lateral wall post-LBBB (lateral post-LBBB 1% SS, all others >5%). In addition, the Commercial method shows greater bias toward high strain values in the septum. Post-LBBB, the difference with MRI-T is increased in all cases except the lateral wall of the Commercial method.

Septal strain patterns and SRS

Figure 4 shows septal wall circumferential strain curves in all canines pre- and post-LBBB. Curves show generally similar patterns with some key differences, particularly post-LBBB. Of the nine post-LBBB canines, seven exhibit LBBB-type septal strain patterns—*i.e.,* double peaked systolic shortening. SRS amplitude varies between methods, most clearly visible in Figure 4 (i, q). The septal flash amplitude varies with the type of regularisation used (Fig. 4n, 4q).

Figure 5 shows Bland-Altman plots of SRS for each STE method compared to MRI-T. Pre-LBBB a solely positive difference is seen, because MRI-T SRS remains at or close to 0, whilst the STE methods estimates of

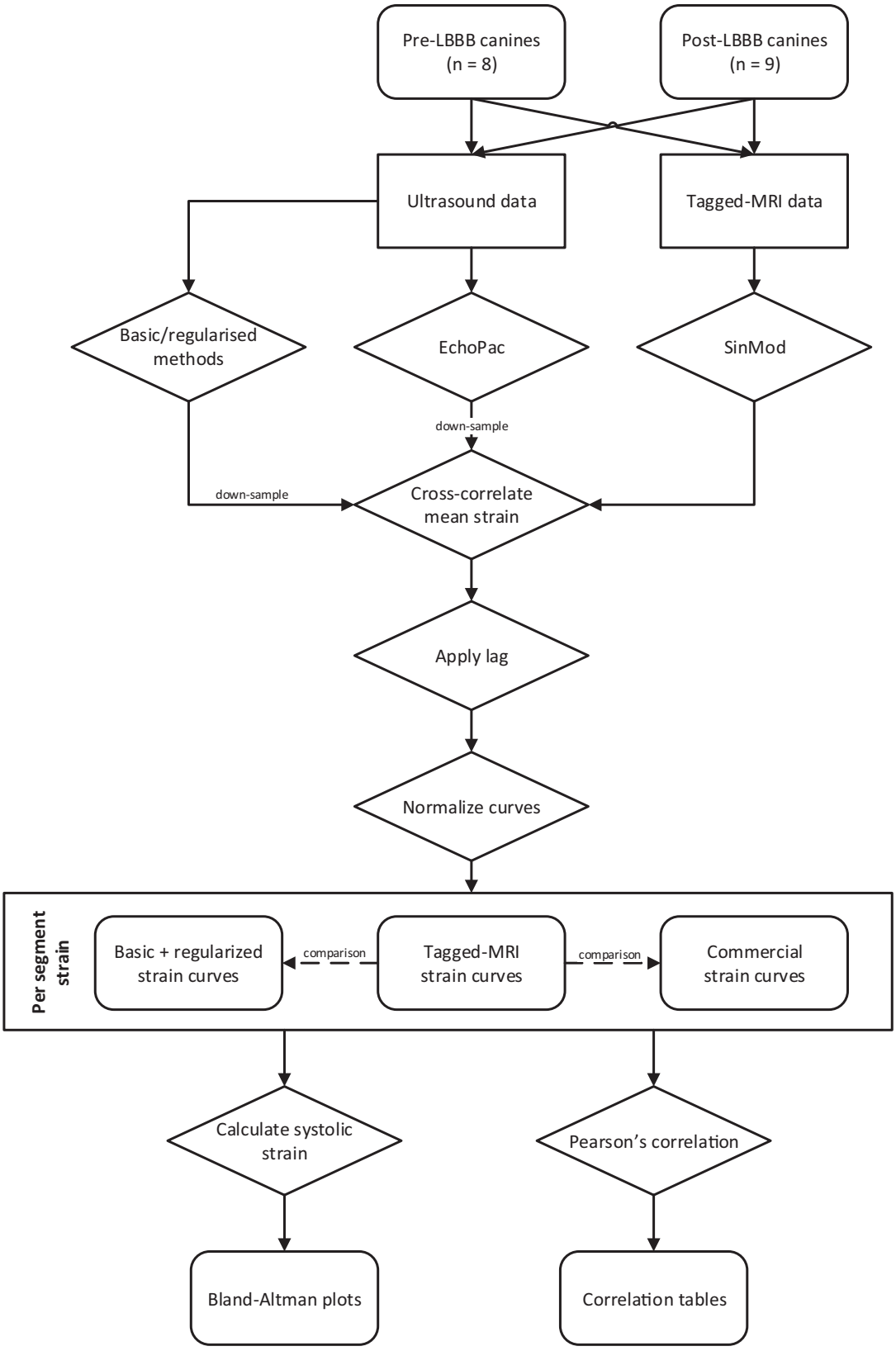

Fig. 2. Flowchart of strain pattern comparison process, resulting in Bland-Altman plots and tables of correlations.

Table 1. Haemodynamic measurements pre-LBBB and post-LBBB

Haemodynamic measurement	Pre-LBBB (n = 8)	Post-LBBB (n = 9)	*p* value
Heart rate (bpm)	96±8	101±23	0.417
Maximum LV dP/dt (mm Hg)	1998±249	1286±296	<0.001
Minimum LV dP/dt (mm Hg)	−2195±177	−1559±362	<0.001
End-systolic pressure (mm Hg)	95±10	83±17	0.017
End-diastolic pressure (mm Hg)	6±2	7±5	0.577
IV mechnical dyssynchrony (ms)	−6±4	−39±10	<0.001
QRS duration (ms)	51±4	102±14	<0.001
LV end-diastolic volume (mL)	56.6±6.0	90.3±29.1	0.121
LV end-systolic volume (mL)	23.1±2.2	43.9±12.6	0.045
LV ejection fraction (%)	59.0±2.7	50.9±5.1	0.026

bpm = beats per minute; LV = left ventricular; IV = interventricular

SRS range from 0%−4.8%. Post-LBBB estimates of SRS vary more between the US methods and MRI-T. In particular, variation is seen depending on the form of regularisation used, as well as the underlying STE software.

Correlation of SRS values between methods (Table 3) showed minor to moderate negative correlation between MRI-T and the STE methods pre-LBBB. However, minor to good correlation was found post-LBBB.

DISCUSSION

This study had two aims: first, to assess the feasibility of using STE-acquired circumferential strain in the assessment of strain patterns pre- and post-LBBB, in a validation against MRI-T; and second, to evaluate different speckle tracking and regularisation methods in the determination of LBBB-type septal strain patterns and parameters. We have shown that circumferential strain curves obtained using different STE methods correlate well with MRI-T, although correlation reduced post-LBBB. Differences were seen on a regional level, based on the type of STE software used. Different forms of regularisation had a minor effect on correlation with MRI-T. All methods exhibited similar LBBB-type patterns in the septal wall post-LBBB, with the type of STE algorithm and regularisation influencing the magnitude of SRS.

Although the measured increase in QRS complex duration obtained *via* ECG in the post-LBBB canines did not satisfy the clinically defined threshold in humans, the QRS duration was significantly increased and represents a severe LBBB in canines.

Comparison of circumferential strain

Overall agreement of normalised circumferential strain patterns obtained with the STE methods and MRI-T was very good, with correlations generally comparable between the Commercial, Basic and regularised methods. Although overestimation was seen in systolic strain, this was consistent across all STE methods. Compared with literature, MRI-T underestimated circumferential strain by 10%−20% (Villarreal et al. 1988). Each STE method correlated excellently with MRI-T in estimating global circumferential strain (GCS) at mid-ventricular level, this agrees with the widespread success of global strain measures (*e.g.,* GLS) in clinical practice (Kalam et al. 2014), because errors in regional strain are averaged out.

Table 2. Median (in bold) and interquartile range (IQR) of correlation between segmental circumferential strain curves for each STE method and MRI-T

	Commercial		Basic		Median		Fourier		Cubic	
Pre-LBBB	Median	IQR	Median	IQR	Median	IQR	Median	IQR	Median	IQR
MA	**0.83**	0.30	**0.90**	0.08	**0.93**	0.08	**0.95**	0.07	**0.96**	0.12
MAL	**0.56**	0.44	**0.89**	0.08	**0.89**	0.09	**0.95**	0.05	**0.92**	0.09
MIL	**0.55**	0.81	**0.94**	0.18	**0.93**	0.21	**0.93**	0.17	**0.90**	0.15
MI	**0.66**	0.42	**0.90**	0.05	**0.90**	0.07	**0.88**	0.14	**0.85**	0.23
MIS	**0.91**	0.10	**0.88**	0.12	**0.89**	0.11	**0.89**	0.08	**0.91**	0.06
MAS	**0.90**	0.10	**0.95**	0.05	**0.95**	0.05	**0.94**	0.04	**0.95**	0.03
Lateral wall	**0.69**	0.45	**0.98**	0.05	**0.98**	0.04	**0.98**	0.08	**0.97**	0.04
Septal wall	**0.94**	0.07	**0.94**	0.06	**0.95**	0.05	**0.96**	0.05	**0.97**	0.05
Avg. all segments	**0.98**	0.02	**0.99**	0.03	**0.99**	0.02	**0.99**	0.02	**0.99**	0.02
Post-LBBB										
MA	**0.75**	0.33	**0.82**	0.28	**0.83**	0.27	**0.91**	0.28	**0.83**	0.22
MAL	**0.69**	0.23	**0.91**	0.17	**0.90**	0.15	**0.90**	0.08	**0.86**	0.13
MIL	**0.65**	0.27	**0.92**	0.10	**0.91**	0.10	**0.92**	0.15	**0.92**	0.11
MI	**0.80**	0.11	**0.84**	0.33	**0.83**	0.32	**0.83**	0.10	**0.76**	0.35
MIS	**0.71**	0.22	**0.73**	0.25	**0.73**	0.30	**0.74**	0.32	**0.75**	0.28
MAS	**0.79**	0.33	**0.81**	0.28	**0.81**	0.28	**0.71**	0.26	**0.83**	0.27
Lateral wall	**0.87**	0.08	**0.95**	0.08	**0.95**	0.06	**0.95**	0.08	**0.93**	0.09
Septal wall	**0.79**	0.19	**0.81**	0.26	**0.82**	0.27	**0.88**	0.26	**0.89**	0.29
Avg. all segments	**0.95**	0.04	**0.95**	0.05	**0.95**	0.05	**0.95**	0.05	**0.96**	0.05

STE = speckle tracking echocardiography; MRI-T = tagged-MRI; IQR = interquartile range; MA = mid-anterior; MAL = mid-anterolateral; MIL = mid-inferolateral; MI = mid-inferior; MIS = mid-inferoseptal; MAS = mid-anteroseptal.

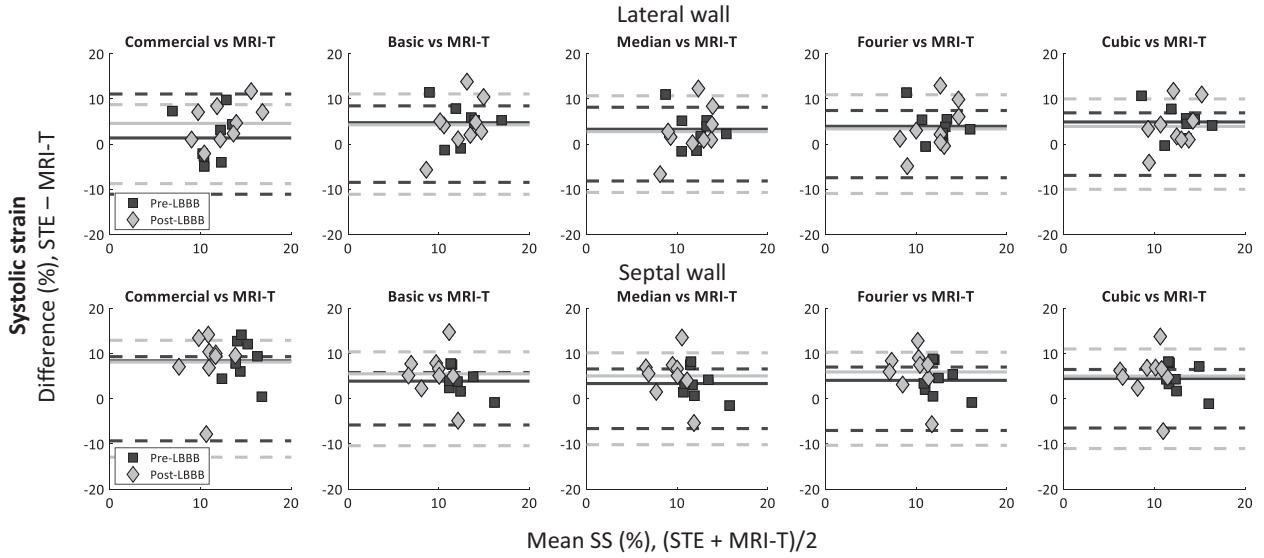

Fig. 3. Bland-Altman plots of mean circumferential systolic strain (SS) pre-LBBB (black) and post-LBBB (grey) comparing STE to MRI-T. Dashed lines represent the 95% confidence interval, whereas the mean difference is represented by the straight lines. STE = speckle tracking echocardiography; MRI-T = tagged MRI; LBBB = left bundle branch block.

Previous studies have compared the results of STE and MRI-T. Amundsen et al. (2006) validated STE, demonstrating its superiority over TDI in non-invasively estimating GLS and GCS. Amzulescu et al. (2017) found good agreement in GLS and GCS, albeit with a significant bias in regional strains, and determined they should not be used clinically. Most recently, van Everdingen et al. (2018) compared strain correlation and different parameters of ventricular discoordination (*i.e.,* SRS), concluding that these parameters showed improved agreement over timing-based parameters of dyssynchrony or regional strain.

These studies identified differences in strain estimation technique, and confounding factors such as mismatched imaging planes, as being an important factor in the agreement of regional strain estimates. The present study's most significant contributions are the investigation into the use of regional circumferential strain and the causes of discrepancies, in particular regularisation, as to our knowledge no study has investigated the issue of regularisation specifically.

In the majority of segments, regularisation did not significantly affect the correlation between MRI-T and our STE implementation. A likely explanation for this is that the regularisation techniques we implemented make use of only information within the US data, meaning the estimated deformation pattern will not significantly differ. The Median regularisation removes outliers during displacement estimation, whilst both Fourier and Cubic regularisation perform spatial and temporal filtering, albeit in different manners. However, some differences were seen between regularisation methods pre- and post-LBBB. This is most prominent for the Fourier method in the septal segments, where correlation was significantly reduced. The Fourier regularisation is applied spatially and temporally, such that the initial geometry is maintained. Post-LBBB non-uniform deformation occurs, particularly in the septum, thereby changing the geometry.

The relatively high US frame rate of 90 frames per second likely led to less pronounced differences between all regularisation techniques, including the commercial software. Part of the rationale for adding regularisation is to counteract the effect of low frame rates, which can result in inaccurate estimation of displacement and therefore inaccurate strain estimates. On the other hand, a high frame rate should not negatively influence regularised strain estimates, given that more data are available from which to determine per frame displacement.

Poor correlation was seen in the lateral wall segments before LBBB induction for the Commercial software. A possible cause of this is the displacement estimation algorithm used by the software: the algorithm focuses on tracking individual bright points within the image. As can be seen in Figure 1d, reflection at the epicardial border leads to a region of very bright speckle next to the lateral wall segment. Although care was taken to place the ROI inward of this bright region, it is possible that the tracking was still influenced. Another possible influence is that the commercial software adjusts the level of spatial and temporal filtering based on (unknown) image quality metrics.

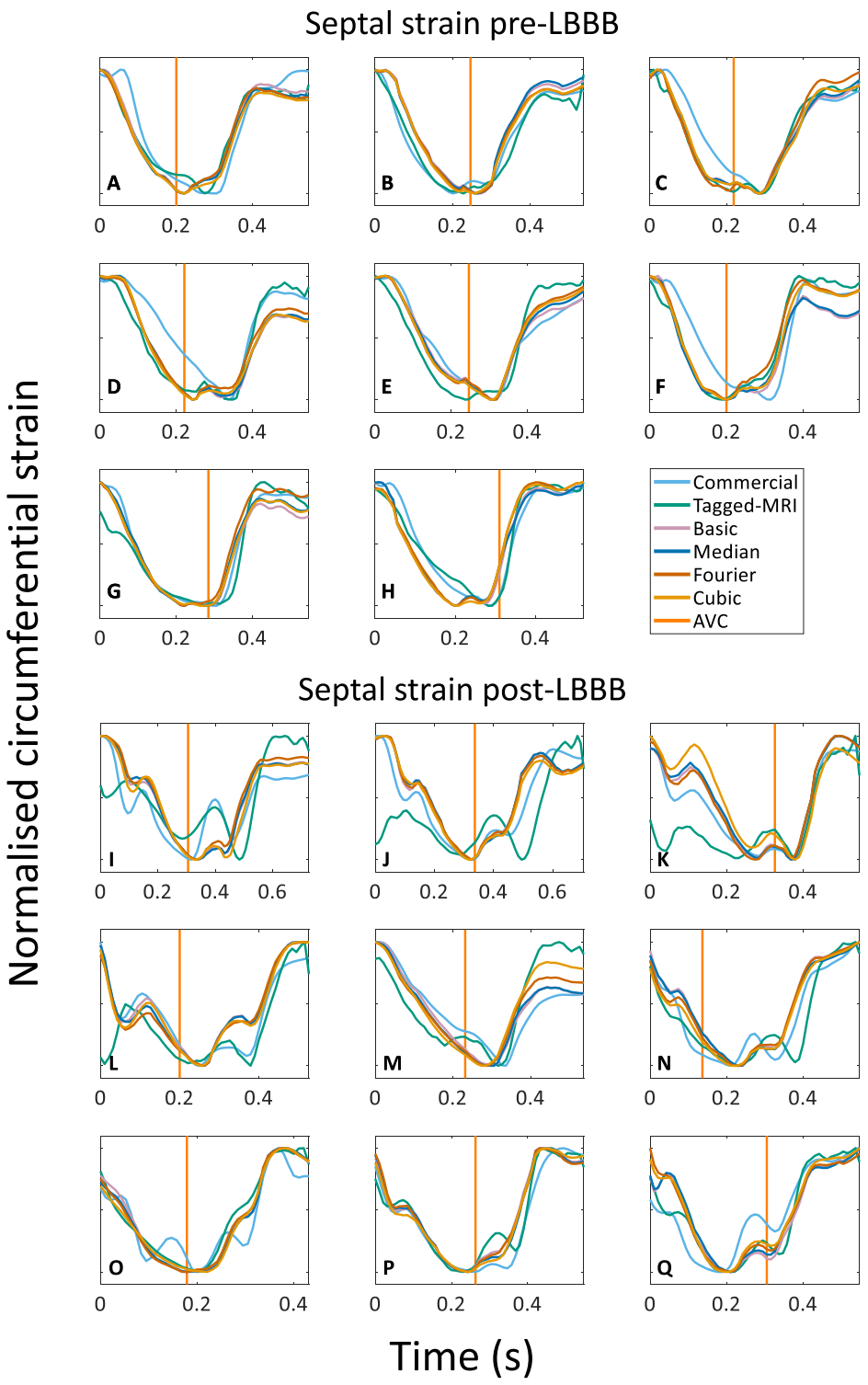

Fig. 4. Aligned and normalized septal wall strain patterns before and after LBBB induction. MRI-T = tagged MRI; LBBB = left bundle branch block; AVC = aortic valve closure.

The limited number of canines with both baseline and LBBB data meant that only statistical comparison between groups was possible, rather than for each canine across the cohort. A possible source of error when comparing MRI-T and STE was a difference in imaging plane. A single imaging plane at mid-ventricular level

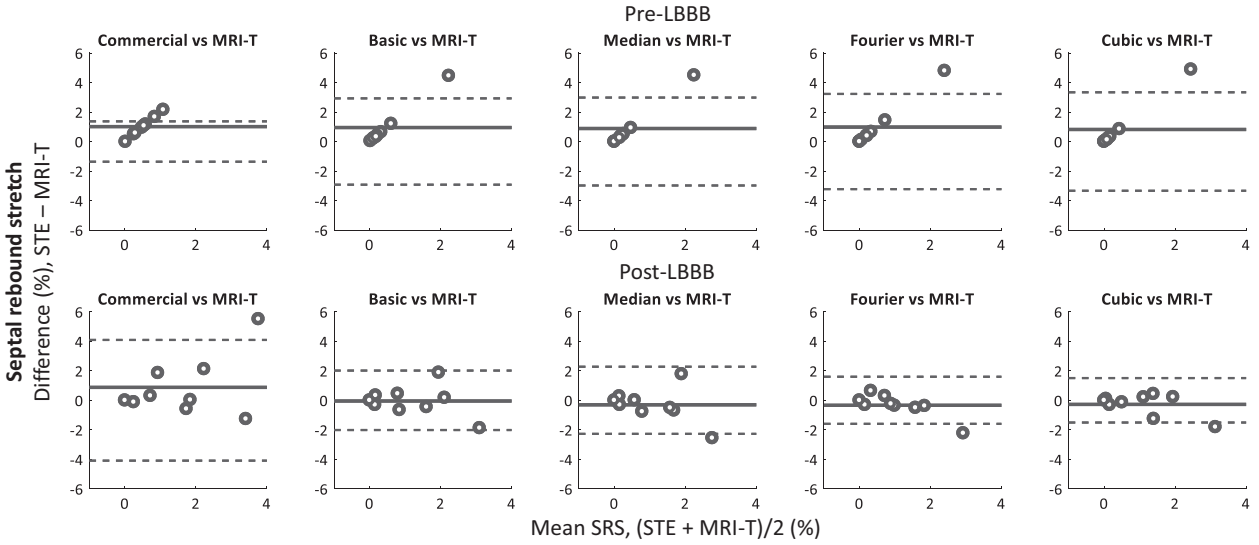

Fig. 5. Bland-Altman plots of septal rebound stretch (SRS) for each method comparing each US method to tagged-MRI (MRI-T). LBBB = left bundle branch block; STE = speckle tracking echocardiography; MRI-T = tagged MRI; SRS = septal rebound stretch; US = ultrasound.

was used in STE analysis, whilst multiple short-axis slices at the mid-ventricular level were used in MRI-T strain estimation. In addition, circumferential strain estimates obtained with STE are more observer specific and less robust than longitudinal strain (Badano et al. 2013, Singh et al. 2010), which could amplify the variability. Last, all images were of a very good quality, which is not guaranteed in clinical US.

Septal strain patterns and SRS

Septal strain patterns were comparable between the methods but with large differences in the degree of septal rebound in some cases. These differences are important due to the septal pattern's possible utility in predicting CRT response (Maréchaux et al. 2014; Risum et al. 2012). We found that estimates of SRS were highly influenced by changes in STE software, similarly to the findings of others (van Everdingen et al. 2017). SRS was more moderately affected by regularisation. The rebound of the septum can be a subtle or abrupt change in deformation pattern, up to 0.5%−7% of total stretch in one or two peaks depending on the type of LBBB (De Boeck et al. 2009). Therefore, accurate motion tracking is susceptible to changes due to filtering, window sizes and other settings. Although regularisation of the Basic method did not bring the results more in line with the Commercial method, this can be explained by the differences in the underlying displacement estimation algorithm.

Table 3. Septal rebound stretch correlation between MRI-T and STE methods

	Commercial	Basic	Median	Fourier	Cubic
Pre-LBBB	−0.609	−0.158	−0.165	−0.128	−0.164
Post-LBBB	0.275	0.646	0.508	0.867	0.822

MRI-T = tagged-MRI; STE = speckle tracking echocardiography.

Clear differences were seen in SRS between MRI-T and the STE methods pre-LBBB: MRI-T estimates were 0% (or effectively 0%), as should be the case before LBBB induction; however, all STE methods estimated an SRS of 0.5% or higher in half of cases. This caused the negative correlation in SRS pre-LBBB and in the majority of cases due to a small septal wall pre-stretch (Fig. 4). Agreement was largely improved post-LBBB, particularly for the Basic/regularised methods. However, non-zero estimates of SRS pre-LBBB are a significant drawback for STE compared with MRI-T.

A cause of the low accuracy of STE in estimating circumferential SRS (and circumferential strain in general) is the lower lateral resolution of US: circumferential deformation of the myocardium in the septal wall occurs across the US lines. Errors due to so-called "peak-hopping" or de-correlation in displacement estimation in the image can propagate and lead to the inaccurate estimation of strain in the lateral direction. Prominent shadowing in the 5 and 7 o'clock regions leads to further decorrelation. Last, attenuation of backscattered US by the circumferential myofibres reduces the overall received signal at the transducer.

The Basic method has previously been validated using *in silico* and *in vitro* phantoms (Lopata et al. 2009). An *in vitro* phantom that would reflect the complex strain pattern seen in hearts with LBBB does not

exist, although an *in silico* phantom could be generated using an electrophysiological cardiac model in combination with US simulation software. The previously acquired data set of a canine LBBB model used in this study was an excellent biological model for the purposes of the present study. LBBB was the only pathology present in the data set, whilst all other conditions were controlled and excellent magnetic resonance and US imagery was obtained.

As we have mentioned, black-box problems are a confounder in studies of different STE software, and may be a cause of the generally low confidence in STE. In order to obtain greater insight into the influence of software, we (or others) would need to implement the displacement estimation algorithms used in the different commercial software packages. Work is being performed by the EACVI/ASE/Industry taskforce to find what differences exist and standardise definitions between vendors (Voigt et al. 2015; D'hooge et al. 2016). However, these studies have, so far, not delved further into the exact methods used by each commercial algorithm. The original basis for the Commercial software (Rappaport et al. 2006) has been published, others have not however, and the algorithm used in recent versions of the software may differ. Implementation of the Commercial method and other vendor's algorithms should yield similar results to the commercial packages themselves. This would therefore be a particularly interesting step to take in future studies, given that we (and others previously) have shown that the type of algorithm and regularisation steps taken can have a significant effect on strain-based parameters of dyssynchrony.

Future work will involve a study in patients using a similar methodology. The study could be further expanded by including additional academic software and implementations of commercial strain estimation software. Given the results of this study, future commercial software should first, disclose the type and degree of regularisation that has occurred when estimating strains; and second, disclose the uncertainty of a measurement, whether due to poor contrast- or signal-to-noise ratio, or other image quality metrics. Furthermore, the release of key information on methods used by speckle tracking algorithms could increase the confidence clinicians have in using STE and accelerate the technique's movement towards day-to-day clinical decision making.

CONCLUSION

We have shown that circumferential strain patterns obtained using commercial and academic STE software agree well with MRI-T. Absolute values showed moderate agreement, with a bias for higher strain from STE. SRS varied with the type of software and extra regularisation applied. Open efforts are needed to understand the underlying causes of differences between STE methods before standardisation can be achieved. This is particularly important given the apparent clinical value of strain-based parameters.

Acknowledgments—Louis S. Fixsen is supported by the European Commission through the H2020 Marie Skłodowska-Curie European Training Network H2020-MSCA-ITN-2014 VPH-CaSE, www.vph-case.eu, GA No. 642612.

REFERENCES

Achilli A, Peraldo C, Sassara M, Orazi S, Bianchi S, Laurenzi F, Donati R, Perego GB, Spampinato A, Valsecchi S, Denaro A, Puglisi A. Prediction of response to cardiac resynchronization therapy: The Selection of Candidates for CRT (SCART) Study. Pacing Clin Electrophysiol 2006;29:S11–S19.

Amundsen BH. It is all about timing! JACC Cardiovasc Imaging 2015;8:158–160.

Amundsen BH, Helle-Valle T, Edvardsen T, Torp H, Crosby J, Lyseggen E, Støylen A, Ihlen H, Lima JAC, Smiseth OA, Slørdahl SA. Noninvasive myocardial strain measurement by speckle tracking echocardiography: Validation against sonomicrometry and tagged magnetic resonance imaging. J Am Coll Cardiol 2006;47:789–793.

Amzulescu MS, Langet H, Saloux E, Manrique A, Boileau L, Slimani A, Allain P, Roy C, de Meester C, Pasquet A, De Craene M, Vancraeynest D, Pouleur AC, Vanoverschelde JLJ, Gerber BL. Head-to-head comparison of global and regional two-dimensional speckle tracking strain versus cardiac magnetic resonance tagging in a multicenter validation study. Circ Cardiovasc Imaging 2017;10 e006530.

Arts T, Prinzen FW, Delhaas T, Milles JR, Rossi AC, Clarysse P. Mapping displacement and deformation of the heart with local sine-wave modeling. IEEE Trans Med Imaging 2010;29:1114–1123.

Badano LP, Cucchini U, Muraru D, Al Nono O, Sarais C, Iliceto S. Use of three-dimensional speckle tracking to assess left ventricular myocardial mechanics: Inter-vendor consistency and reproducibility of strain measurements. Eur Heart J Cardiovasc Imaging 2013;14:285–293.

Brignole M, Auricchio A, Baron-Esquivias G, Bordachar P, Boriani G, Breithardt OA, Cleland J, Deharo JC, Delgado V, Elliott PM, Gorenek B, Israel CW, Leclercq C, Linde C, Mont L, Padeletti L, Sutton R, Vardas PE. 2013 ESC Guidelines on cardiac pacing and cardiac resynchronization therapy. Europace 2013;15:1070–1118.

Bunting E, Lambrakos L, Kemper P, Whang W, Garan H, Konofagou E. Imaging the propagation of the electromechanical wave in heart failure patients with cardiac resynchronization therapy. Pacing Clin Electrophysiol 2016;40:35–45.

Chung ES, Leon AR, Tavazzi L, Sun J-P, Nihoyannopoulos P, Merlino J, Abraham WT, Ghio S, Leclercq C, Bax JJ, Yu C-M, Gorcsan J, St John Sutton M, De Sutter J, Murillo J. Results of the Predictors of Response to CRT (PROSPECT) trial. Circulation 2008;117:2608–2616.

D'Andrea A, Caso P, Scarafile R, Riegler L, Salerno G, Castaldo F, Gravino R, Cocchia R, Del Viscovo L, Limongelli G, Di Salvo G, Ascione L, Iengo R, Cuomo S, Santangelo L, Calabrò R. Effects of global longitudinal strain and total scar burden on response to cardiac resynchronization therapy in patients with ischaemic dilated cardiomyopathy. Eur J Heart Failure 2009;11:58–67.

De Boeck BW, Teske AJ, Meine M, Leenders GE, Cramer MJ, Prinzen FW, Doevendans PA. Septal rebound stretch reflects the functional substrate to cardiac resynchronization therapy and predicts volumetric and neurohormonal response. Eur J Heart Failure 2009;11:863–871.

D'hooge J, Barbosa D, Gao H, Claus P, Prater D, Hamilton J, Lysyansky P, Abe Y, Ito Y, Houle H, Pedri S, Baumann R, Thomas J, Badano LP. Two-dimensional speckle tracking echocardiography: Standardization efforts based on synthetic ultrasound data. Eur Heart J Cardiovasc Imaging 2016;17:693–701.

Ghani A, Delnoy PP, Adiyaman A, Ottervanger JP, Ramdat Misier AR, Smit JJ, Elvan A. Response to cardiac resynchronization therapy as

assessed by time-based speckle tracking imaging. Pacing Clin Electrophysiol 2015;38:455–464.
Han Y, Chan J, Haber I, Peters DC, Zimetbaum PJ, Manning WJ, Yeon SB. Circumferential myocardial strain in cardiomyopathy with and without left bundle branch block. J Cardiovasc Magn Reson 2010;12:2.
Helm RH, Leclercq C, Paris OP, Ozturk C, McVeigh E, Lardo AC, Kass DA. Cardiac dyssynchrony analysis using circumferential versus longitudinal strain: Implications for assessing cardiac resynchronization. Circulation 2005;111:2760–2767.
Holzmeister J, Leclercq C. Implantable cardioverter defibrillators and cardiac resynchronisation therapy. Lancet 2011;378:722–730.
Kalam K, Otahal P, Marwick TH. Prognostic implications of global LV dysfunction: A systematic review and meta-analysis of global longitudinal strain and ejection fraction. Heart 2014;100:1673–1680.
Kirn B, Jansen A, Bracke F, van Gelder B, Arts T, Prinzen FW. Mechanical discoordination rather than dyssynchrony predicts reverse remodeling upon cardiac resynchronization. Am J Physiol Heart Circ Physiol 2008;295:H640–H646.
Lopata RGP, Nillesen MM, Hansen HHG, Gerrits IH, Thijssen JM, de Korte CL. Performance evaluation of methods for two-dimensional displacement and strain estimation using ultrasound radio frequency data. Ultrasound Med Biol 2009;35:796–812.
Maréchaux S, Guiot A, Castel AL, Guyomar Y, Semichon M, Delelis F, Heuls S, Ennezat PV, Graux P, Tribouilloy C. Relationship between two-dimensional speckle-tracking septal strain and response to cardiac resynchronization therapy in patients with left ventricular dysfunction and left bundle branch block: A prospective pilot study. J Am Soc Echocardiogr 2014;27:501–511.
McMurray JJV, Adamopoulos S, Anker SD, Auricchio A, Bohm M, Dickstein K, Falk V, Filippatos G, Fonseca C, Gomez-Sanchez MA, Jaarsma T, Kober L, Lip GYH, Maggioni AP, Parkhomenko A, Pieske BM, Popescu BA, Ronnevik PK, Rutten FH, Schwitter J, Seferovic P, Stepinska J, Trindade PT, Voors AA, Zannad F, Zeiher A, Bax JJ, Baumgartner H, Ceconi C, Dean V, Deaton C, Fagard R, Funck-Brentano C, Hasdai D, Hoes A, Kirchhof P, Knuuti J, Kolh P, McDonagh T, Moulin C, Popescu BA, Reiner Z, Sechtem U, Sirnes PA, Tendera M, Torbicki A, Vahanian A, Windecker S, McDonagh T, Sechtem U, Bonet LA, Avraamides P, Ben Lamin HA, Brignole M, Coca A, Cowburn P, Dargie H, Elliott P, Flachskampf FA, Guida GF, Hardman S, Iung B, Merkely B, Mueller C, Nanas JN, Nielsen OW, Orn S, Parissis JT, Ponikowski P. ESC guidelines for the diagnosis and treatment of acute and chronic heart failure 2012: The Task Force for the Diagnosis and Treatment of Acute and Chronic Heart Failure 2012 of the European Society of Cardiology. Developed in collaboration with the Heart. Eur Heart J 2012;33:1787–1847.
Moen CA, Salminen P-R, Dahle GO, Hjertaas JJ, Grong K, Matre K. Is strain by speckle tracking echocardiography dependent on user controlled spatial and temporal smoothing? An experimental porcine study. Cardiovascular Ultrasound 2013;11:32.
Pollock DSG. Smoothing with cubic splines. Handbook of Time Series Analysis, Signal Processing, and Dynamics. London: Academic Press; 1999. p. 293–322.
Prinzen FW, Hunter WC, Wyman BT, McVeigh ER. Mapping of regional myocardial strain and work during ventricular pacing: Experimental study using magnetic resonance imaging tagging. J Am Coll Cardiol 1999;33:1735–1742.
Rappaport D, Adam D, Lysyansky P, Riesner S. Assessment of myocardial regional strain and strain rate by tissue tracking in B-mode echocardiograms. Ultrasound Med Biol 2006;32:1181–1192.
Risum N, Jons C, Olsen NT, Fritz-Hansen T, Bruun NE, Hojgaard MV, Valeur N, Kronborg MB, Kisslo J, Sogaard P. Simple regional strain pattern analysis to predict response to cardiac resynchronization therapy: Rationale, initial results, and advantages. Am Heart J 2012;163:697–704.
Singh GK, Cupps B, Pasque M, Woodard PK, Holland MR, Ludomirsky A. Accuracy and reproducibility of strain by speckle tracking in pediatric subjects with normal heart and single ventricular physiology: A two-dimensional speckle-tracking echocardiography and magnetic resonance imaging correlative study. J Am Soc Echocardiogr 2010;23:1143–1152.
Strik M, van Middendorp LB, Houthuizen P, Ploux S, van Hunnik A, Kuiper M, Auricchio A, Prinzen FW. Interplay of electrical wavefronts as determinant of the response to cardiac resynchronization therapy in dyssynchronous canine hearts. Circ Arrhythm Electrophysiol 2013;6:924–931.
van Everdingen WM, Maass AH, Vernooy K, Meine M, Allaart CP, De Lange FJ, Teske AJ, Geelhoed B, Rienstra M, Van Gelder IC, Vos MA, Cramer MJ. Comparison of strain parameters in dyssynchronous heart failure between speckle tracking echocardiography vendor systems. Cardiovascular Ultrasound 2017;15:25.
van Everdingen WM, Zweerink A, Nijveldt R, Salden OAE, Meine M, Maass AH, Vernooy K, De Lange FJ, van Rossum AC, Croisille P, Clarysse P, Geelhoed B, Rienstra M, Van Gelder IC, Vos MA, Allaart CP, Cramer MJ. Comparison of strain imaging techniques in CRT candidates: CMR tagging, CMR feature tracking and speckle tracking echocardiography. Int J Cardiovasc Imaging 2018;34:443–456.
Verbeek XA, Vernooy K, Peschar M, Van der Nagel T, Van Hunnik A, Prinzen FW. Quantification of interventricular asynchrony during LBBB and ventricular pacing. Am J Physiol Heart Circ Physiol 2002;283:H1370–H1378.
Villarreal FJ, Waldman LK, Lew WY. Technique for measuring regional two-dimensional finite strains in canine left ventricle. Circ Res 1988;62:711–721.
Voigt JU, Pedrizzetti G, Lysyansky P, Marwick TH, Houle H, Baumann R, Pedri S, Ito Y, Abe Y, Metz S, Song JH, Hamilton J, Sengupta PP, Kolias TJ, D'Hooge J, Aurigemma GP, Thomas JD, Badano LP. Definitions for a common standard for 2D speckle tracking echocardiography: Consensus document of the EACVI/ASE/Industry Task Force to standardize deformation imaging. Eur Heart J Cardiovasc Imaging 2015;16:1–11.